



# A Multi-phasic Approach for Estimating the Biot Coefficient for Grimsel Granite

Patrick Selvadurai<sup>a,\*</sup>, Paul Selvadurai<sup>b,\*\*</sup>, Morteza Nejati<sup>b,\*\*</sup>

<sup>a</sup>Department of Civil Engineering and Applied Mechanics, McGill University, Montréal, QC, Canada H3A 0C3

<sup>b</sup>Department of Earth Sciences, ETH Zurich, Switzerland

## Abstract

This paper presents an alternative approach for estimating the Biot coefficient for the Grimsel granite, which appeals to the multi-phasic mineralogical composition of the rock. The modelling considers the transversely isotropic nature of the rock that is evident from both the visual appearance of the rock and determined from mechanical testing. Conventionally, estimation of the compressibility of the solid material is performed by fluid saturation of the pore space and pressurization. The drawback of this approach in terms of complicated experimentation and influences of the unsaturated pore space is alleviated by adopting the methods for estimating the solid material compressibility using developments in theories of multiphase materials. The results of the proposed approach are compared with estimates available in the literature.

**Keywords:** Biot coefficient, transversely isotropic rocks, compressibility of the solid materials, Hashin-Rosen estimates, Voigt-Reuss-Hill estimates

## 1. Introduction

The classical theory of poroelasticity proposed by Biot (1941) is a major contribution to the disciplines of geosciences and geomechanics with applications that include porous earth materials saturated by fluids. The studies in this area are numerous and no attempt will be made to provide a comprehensive survey of past and recent developments. Advances in the area of poroelasticity, and its applications to problems in geomechanics in particular are given by Rice and Cleary (1976); Yue and Selvadurai (1995); Selvadurai (1996, 2007); Wang (2000); Verruijt (2015); Cheng (2015); Selvadurai et al. (2015); Selvadurai and Suvorov (2016) and others. The basic development of the classical theory of poroelasticity relies on constitutive assumptions of Hookean elastic behaviour of the porous skeleton and Darcy flow through the porous medium. In addition, an important component of the theory relates to the partitioning of the total stress tensor for the poroelastic solid between the stresses carried purely by the porous skeleton and the stresses carried by the pore fluid. The partitioning is an important component in the theory of poroelasticity that allows the time-dependent shedding of the applied stresses from the pore fluid to the porous skeleton. The stresses sustained by the porous skeleton have important consequences to the definition of failure of the poroelastic material either through the development of damage (Selvadurai, 2004; Selvadurai and Shirazi, 2004, 2005; Selvadurai et al., 2015), or fracture development and boundary effects on heterogeneities (Selvadurai et al., 2011; Selvadurai and Głowacki, 2017, 2018) or plastic flow (Selvadurai and Suvorov, 2012, 2014). From an environmental geosciences perspective, alterations in

\*Corresponding author, William Scott Professor and Distinguished James McGill Professor

\*\*Post-Doctoral Fellow

Email address: patrick.selvadurai@mcgill.ca (Patrick Selvadurai)



24 the skeletal permeability associated with its damage can lead to enhanced migration of contaminants and hazardous  
25 materials. In Biot's theory, the partitioning of the total stress is achieved through consideration of the bulk modulus  
26 of the porous skeleton ( $K_D$ ) and the bulk modulus of the solid material composing the porous skeleton ( $K_S$ ), which  
27 introduces the Biot coefficient  $\alpha$  and for an isotropic elastic skeleton, has the form  $\alpha = 1 - (K_D/K_S)$ . When the bulk  
28 modulus of the solid material is large in comparison to the skeletal bulk modulus,  $\alpha \rightarrow 0$ , which is the conventional  
29 stress partitioning approach proposed in the theory of soil consolidation proposed by Terzaghi (1923). Unlike in soils,  
30 the Biot coefficient for rocks can be less than unity. If Biot's classical theory of poroelasticity is accepted, values of  $\alpha$   
31 cannot be greater than unity. Such a value would imply that either  $K_D < 0$  or  $K_S < 0$ , which would violate the positive  
32 definiteness arguments for the strain energy of an elastic porous skeleton (Davis and Selvadurai, 1996; Selvadurai,  
33 2000) with no locked-in self equilibrating stresses (i.e. the skeleton expands under compressive isotropic stresses). A  
34 range of values for  $\alpha$  is given by Detournay and Cheng (1993); Wang (2000); Cheng (2015).

35 The experimental procedure for determining the Biot coefficient  $\alpha$  involves estimating the bulk modulus of the  
36 porous skeleton ( $K_D$ ), which, in the case of an isotropic skeletal fabric, can be obtained by subjecting a dry or mois-  
37 ture free and jacketed specimen of the rock to isotropic compression and measuring the resulting volumetric strain.  
38 This is a straightforward experimental technique and the results can also be verified by conducting uniaxial compression  
39 tests on the isotropic rock and measuring both the Young's modulus and Poisson's ratio. The measurement of  
40 the compressibility of the solid material composing the skeletal fabric can be either straightforward or complicated  
41 depending on the permeability characteristics of the porous material. For rocks with relatively high permeability (e.g.  
42 Indiana limestone  $10^{-13} \sim 10^{-15} \text{m}^2$  (Selvadurai and Glowacki, 2008; Selvadurai and Selvadurai, 2010, 2014), Vosges  
43 sandstone  $\sim 10^{-13} \text{m}^2$  (Moulu et al., 1997), etc.), the pore space of the rock can be saturated by initiating a combination  
44 of steady flow and vacuum saturation. To determine the compressibility of the solid material, the confining isotropic  
45 stresses are allowed to nearly equilibrate with the pore fluid pressure and the volume changes measured can be used to  
46 estimate the compressibility of the solid material composing the porous fabric. With very low permeability materials  
47 (e.g. the Cobourg limestone  $\sim 10^{-23} \text{m}^2$  to  $10^{-19} \text{m}^2$  (Selvadurai et al., 2011)), the process of saturation of the pore  
48 space can take an inordinately long time with no assurance that the entire pore space is fully saturated or that there are  
49 no residual pore fluid pressure artifacts (Selvadurai, 2009). Furthermore, even if the pore space is saturated, attain-  
50 ing equalization of the externally applied pressure with the internal pore fluid pressure can take substantial time (for  
51 150 mm diameter cylindrical Cobourg limestone samples, more than 100 days are required for saturation). For this  
52 reason, Selvadurai (2018) proposed an alternative approach where the compressibility of the solid material phase(s)  
53 can be estimated by considering the multi-phasic theories developed for estimating the effective properties of composite  
54 elastic materials. The composite material theories associated with the Voigt-Reuss-Hill estimates (Voigt, 1928;  
55 Reuss, 1929; Hill, 1952, 1965) and the upper and lower bound estimates proposed by Hashin and Shtrikman (1963)  
56 can be used to estimate the bulk modulus of the solid material (see also Walpole, 1966; Francfort and Murat, 1986).  
57 In this paper, we apply these basic concepts to determine the Biot coefficient for the Grimsel granite. This granite is  
58 encountered in the Underground Research Laboratory constructed in Grimsel, Switzerland, in order to perform heater  
59 experiments to simulate the thermo-hydro-mechanical (THM) loading associated with heat-emitting containers in the  
60 event that the site is chosen as a repository for the deep geologic disposal of high level nuclear fuel waste (i.e. the  
61 Full-scale Engineered Barriers EXperiment (FEBEX).) A typical section along the Grimsel Laboratory associated  
62 with the FEBEX heater experiment location is shown in Figure 1.

63 The Aar granitic rock (also referred to as Aare granitic rock) setting at Grimsel has been associated with initiatives  
64 related to the use of granitic rock formations as potential hosts for the creation of deep geologic repositories for the

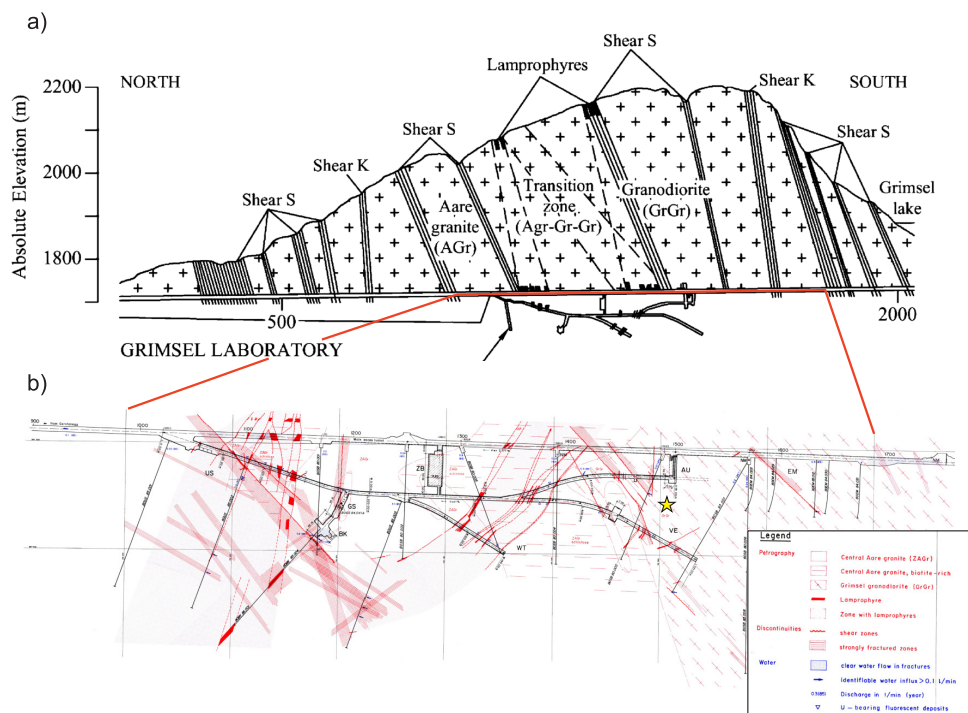


Figure 1: (a) The Grimsel Laboratory and the FEBEX Drift [After Alonso et al. (2005)]; (b) Detailed map view of the FEBEX drift for reference only [After Keusen et al. (1989) and from NAGRA Technical Report NTB87-14E].

65 disposal of heat-emitting nuclear fuel waste. Detailed descriptions of the geological settings of the Aar massif of  
 66 the Central Alps are given by several authors including Stalder (1964); Wüthrich (1965); Steck and Burri (1971);  
 67 Schaltegger (1990b,a); Schaltegger and Corfu (1992) and references to further studies are given by Goncalves et al.  
 68 (2012). Geoscientific studies of the Aar granite have been conducted by a number of agencies including NAGRA  
 69 and ENRESA and these initiatives are documented in several reports and articles by Amiguet (1985); Pahl et al.  
 70 (1989); Keusen et al. (1989); Möri et al. (2003); Alonso and Alcoverro (2005); Alonso et al. (2005); Rabung et al.  
 71 (2012); Bouffier (2015); Garralón et al. (2017); Krietsch et al. (2019). In relation to the FEBEX research experiments,  
 72 the geological setting of the Grimsel Laboratory contains alternate layers of the Aar granite, transition zones and  
 73 Granodiorite, separated by Lamprophyres and zones that are subjected to intense shearing. A typical view of the  
 74 geological setting is shown in Figure 1. During the FEBEX experiments, the Grimsel Laboratory was used to conduct  
 75 heater experiments where the heaters were encapsulated in bentonitic clay. An extensive program of research was  
 76 conducted by a series of research groups to validate the THM response of both the bentonitic buffer and the rock mass  
 77 and the results of the research efforts are documented by Alonso and Alcoverro (2005) and Alonso et al. (2005). The  
 78 Grimsel granite used in this research investigation was obtained from boreholes PRP16.001 and INJ16.001 located in  
 79 the southern part of the laboratory, drilled from the AU cavern. These boreholes were drilled as a part of the Grimsel



80 In-situ Stimulation and Circulation (ISC) project (see the location in Figure 1) that investigated the seismo-hydro-  
 81 mechanical response of the rock mass to hydraulic stimulation (Amann et al., 2018; Gischig et al., 2018; Doetsch  
 82 et al., 2018; Jalali et al., 2018).

83 During the geological evolution of the Aar Massif, the strata acquired different mineralogical compositions and  
 84 the studies by Schaltegger and Krähenbühl (1990) contain very detailed evaluations of the mineralogical composi-  
 85 tions of rocks recovered from the Grimsel and Reuss regions. This information is valuable for estimating the solid  
 86 material compressibility of the Grimsel granite and for distinguishing the sample locations. For example, the work of  
 87 Jokelainen et al. (2013) provides information on the mineralogical composition of the Grimsel granodiorite and the  
 88 study by Missana and Garcia-Gutiérrez (2012) provides the mineralogical composition of the FEBEX granite. The  
 89 results reported in these investigations are summarized in Tables 1-4 for completeness.

Table 1: Short Petrographical Descriptions of the Rock Samples Analyzed by Schaltegger and Krähenbühl (1990). Compositions are estimated from thin section, all=allanite; ap=apatite; bio=biotite; cc=calcite; chl=chlorite; ep=epidote; fluo=fluorite; gar=garnet; kfs=K-feldspar; leuc=leucoxene; op=opaque; plag=plagioclase; ser=sericite; sph=sphene; stlp = stilpnomelane; qtz = quartz; zir = zircon.

Sample No.	Rock Name	Mesoscopic description	Mineralogical composition
KAW 128	Northern Border Facies, Gurtellen granite (Reuss valley)	leucocratic, massiv, coarse-grained granite	38% qtz, 35% kfs, 25% plag, 2% bio; ap, op, all, zir, gar, sph, ep, stlp, chl;
KAW 2213A	Grimsel Granodiorite Grimsel lake (Grimsel)	dark, coarse-grained granite to granodiorite, strongly foliated in most cases, augen texture; abundant dark enclaves	25% qtz, 25% kfs, 38% plag, 12%; bio; ap, op, sph, all, zir, chl, ep, ser, leuc, cc; plag cumulates
KAW 2219	Central Aar Granite s.s., main facies, Chuenzentennen (Grimsel)	coarse-grained granite with only slight cataclastic deformation	32% qtz, 29% kfs, 31% plag, 8% bio; ap, op, zir, all, leuc, chl, ser, ep
KAW 2220	Central Aar Granite s.s., leucocratic facies, Hangholz (Grimsel)	medium-grained granite, slightly foliated, occurring as stocks and schlieren within the main facies of the Central Aar Granite s.s.	34% qtz, 32% kfs, 28% plag, 6% bio; ap, op, zir, all, gar, chl, leuc, ser, ep
KAW 2408	Mittagflue Granite, Tschingel bridge (Grimsel)	leucocratic, massive, coarse-grained granite, analogous to the Northern Border Facies of the Reuss valley	35% qtz, 35% kfs, 28% plag, 2% bio; ap, zir, gar, all, chl, ep, stlp
KAW 2427	Central Aar Granite s.s., main facies, Gelmerstutz (Grimsel)	coarse-grained, massive granite	main rock-forming minerals as KAW 2219, op, all, sph, zir, ap, ep, ser
KAW 2518	Central Aar Granite s.l., Göschenen (Reuss valley)	leucocratic, medium-grained granite, massive to slightly foliated	32% qtz, 32% kfs, 32% plag, 4% bio; ap, ep, all, zir, gar, ser, leuc
KAW 2519	Central Aar Granite s.l., Schöllenen (Reuss valley)	dark, coarse-grained granodiorite with moderate foliation, augen texture	27% qtz, 35% plag, 28% kfs, 10% bio; all, zir, op, ap, sph, ep, leuc, chl
KAW 2521	Central Aar Granite s.l. Schöllenen (Reuss valley)	coarse-grained granodiorite, strongly foliated, similar to KAW 2519	zir, op, ap, sph, ep, leuc, chl same rock-forming minerals as KAW 2519
KAW 2529	Kessiturm Aplite, white facies (Grimsel)	fine-grained, aplitic (leucogranitic) intrusion of 200 × 800 m within the Grimsel Granodiorite	40% qtz, 35% kfs, 24% plag, 1% bio; zir, gar, op, fluo, leuc, chl, ep
KAW 2532	Kessiturm Aplite, grey facies (Grimsel)	fine-grained grey aplite, forming blobs and schlieren within the white Kessiturm aplite	40% qtz, 30% kfs, 28% plag, 2% bio; gar, chl, ep, ser

90 Figure 2 shows cores of the Grimsel granite and, from a visual perspective, the rock has the appearance of strati-  
 91 fications that would point to the likely presence of transverse isotropy, in terms of its elasticity properties, fluid flow  
 92 and fracture and failure characteristics.

93 The microstructure includes larger crystals of quartz (with dimensions up to 8 mm) and this requires that a suitable  
 94 representative volume element is considered, both in the mechanical testing and mineralogical property evaluations.



Table 2: Geochemical Descriptions of the Rock Samples Across the Grimsel Test Site given by Keusen et al. (1989).

	Central Aare granite					Grimsel-Granodiorite					
	SB1	SB2	SB2	SB3	SB4	SB5	SB5	SB6	SB6	SB6	SB5
	74.98	14.00	74.00	93.00	72.20	35.96	39.20	48.98	59.00	75.97	39.20
	Wt.%	Wt.%	Wt.%	Wt.%	Wt.%	Wt.%	Wt.%	Wt.%	Wt.%	Wt.%	Wt.%
SiO <sub>2</sub>	74.65	69.56	74.67	68.65	71.22	67.95	67.76	69.9	65.35	66.57	66.66
TiO <sub>2</sub>	0.2	0.41	0.16	0.42	0.41	0.58	0.61	0.44	0.51	0.56	0.47
Al <sub>2</sub> O <sub>3</sub>	13.14	14.72	12.78	15.21	13.88	15.04	15.2	14.48	17.03	16.1	14.73
Fe <sub>2</sub> O <sub>3</sub>	1.39	2.98	1.13	2.97	2.6	3.44	3.58	2.71	3.3	3.61	4.1
MnO	0.04	0.1	0.04	0.09	0.07	0.07	0.07	0.06	0.08	0.08	0.09
MgO	0.24	0.69	0.18	0.69	0.56	1.27	0.54	0.76	0.91	0.88	0.12
CaO	1.01	2.08	0.93	1.97	1.84	1.85	1.29	1.71	2.56	2.83	6.99
Na <sub>2</sub> O	3.88	4.52	3.69	4.59	3.87	4.01	4.57	3.98	4.9	4.84	3.95
K <sub>2</sub> O	4.7	3.47	4.83	4.03	3.91	4.03	3.77	4.59	3.56	3.35	1.57
P <sub>2</sub> O <sub>5</sub>	0.07	0.13	0.05	0.13	0.12	0.19	0.19	0.14	0.16	0.18	0.15
Cr <sub>2</sub> O <sub>3</sub>	< 0.01	< 0.01	< 0.01	< 0.01	< 0.01	< 0.01	< 0.01	< 0.01	< 0.01	< 0.01	< 0.01
NiO	0.01	0.01	0.01	0.01	0.01	0.01	0.01	0.01	0.01	0.01	0.01
Loss of ign.	0.31	0.49	0.38	0.6	0.53	0.81	0.78	0.45	0.84	0.6	0.69
Ignition	98.92	99.15	98.84	99.35	99.01	99.24	99.36	99.22	99.2	99.6	99.52

Table 3: Mineralogical composition of the Grimsel Granodiorite (Gr-Gr) [After Jokelainen et al. (2013)].

Mineral	Sample 1 (Volume %)	Sample 2 (Volume %)
Plagioclase	39.0	34.0
Quartz	28.4	37.2
K-Feldspar	21.6	12.8
Biotite	5.0	7.8
Muscovite + sericite	2.6	1.6
Epidote	1.2	1.0
Amphibole	1.8	4.6
Chlorite	0.2	0.4
Titanate	-	0.6
Opaque minerals	0.2	-

95 Extensive geomechanical characterization studies have been performed on the Grimsel granite and these are given  
 96 in the references cited previously. Permeability studies are also reported by Schild et al. (2001). A comprehensive  
 97 inter-laboratory study of permeability of the Grimsel granodiorite is also given in David et al. (2018a,b).

98 The objective of this study is to employ the existing data on the mechanical characterization of the transversely  
 99 isotropic granite to estimate the skeletal compressibility of the granite and to use XRD studies of the mineralogical  
 100 composition of the Grimsel granite to estimate the compressibility of the solid phase composing the porous fabric.

## 101 2. Skeletal Bulk Modulus of the Grimsel Granite

102 The fabric of the Grimsel granite is indicative of a transversely isotropic material (Nejati, 2018; Dutler et al., 2018;  
 103 Dambly et al., 2019; Nejati et al., 2019). The elastic stress-strain relationships for a transversely isotropic material  
 104 can be expressed in several forms (see e.g. Hearmon, 1961; Lekhnitskii, 1963; Ting, 1996). We consider the case  
 105 where the plane of isotropy ( $x, y$ ) of the transversely isotropic elastic material is normal to the  $z$ -axis. The equations  
 106 of elasticity governing the normal strains can be written in the forms



Table 4: Mineralogical composition of the FEBEX Granite [After Missana and Garcia-Gutiérrez (2012)].

Mineral	Volume (%)
Quartz	30-36
Plagioclase/Albite	19-23
K-Feldspar	31-37
Biotite-Chlorite	6-8
Muscovite	1-2



Figure 2: The Grimsel granite cores.

$$\begin{aligned}
 \epsilon_{xx} &= \frac{\sigma_{xx}}{E_x} - \frac{\nu_{yx}\sigma_{yy}}{E_y} - \frac{\nu_{zx}\sigma_{zz}}{E_z} \\
 \epsilon_{yy} &= -\frac{\nu_{xy}\sigma_{xx}}{E_x} + \frac{\sigma_{yy}}{E_y} - \frac{\nu_{zy}\sigma_{zz}}{E_z} \\
 \epsilon_{zz} &= -\frac{\nu_{xz}\sigma_{xx}}{E_x} - \frac{\nu_{yz}\sigma_{yy}}{E_y} + \frac{\sigma_{zz}}{E_z}
 \end{aligned} \tag{1}$$

107 We point out that the Poisson's ratio is generally defined as  $\nu_{ij} = -\epsilon_j/\epsilon_i$  for a stress in the  $i$  direction. From Betti's  
 108 reciprocal theorem,

$$\frac{\nu_{xy}}{E_x} = \frac{\nu_{yx}}{E_y}, \quad \frac{\nu_{xz}}{E_x} = \frac{\nu_{zx}}{E_z}, \quad \frac{\nu_{yz}}{E_y} = \frac{\nu_{zy}}{E_z} \tag{2}$$

109 Due to the isotropic behaviour in the  $xy$  plane,  $E_x = E_y$ , and  $\nu_{zy} = \nu_{zx}$ . These relations reduce the independent  
 110 material constants needed to define the principal strains to four:  $E_x$ ,  $E_z$ ,  $\nu_{xy}$  and  $\nu_{zx}$ . Consider the situation where an  
 111 element of the transversely isotropic elastic medium is subjected to an isotropic compressive stress state:  $\sigma_{xx} = \sigma_{yy} =$   
 112  $\sigma_{zz} = p$ . The infinitesimal volumetric strain

$$\epsilon_v = \epsilon_{xx} + \epsilon_{yy} + \epsilon_{zz} = p \left[ \frac{2}{E_x} (1 - \nu_{xy}) + \frac{1}{E_z} (1 - 4\nu_{zx}) \right] \tag{3}$$

113 The skeletal bulk modulus for the transversely isotropic elastic material can be expressed in the form

$$K_D^{\text{TI}} = \frac{p}{\epsilon_v} = \frac{E_x E_z}{2E_z(1 - \nu_{xy}) + E_x(1 - 4\nu_{zx})} \tag{4}$$

114 In terms of the elasticity parameters that are applicable to the direction normal to the planes of stratification ( $N$ )  
 115 and directions along the planes of foliation or stratification ( $T$ ), Eq. (4) can be written as



$$K_D^{\text{TI}} = \frac{E_T E_N}{2E_N(1 - \nu_{TT}) + E_T(1 - 4\nu_{NT})} \quad (5)$$

116 In the limit of material isotropy,  $E_N = E_T = E$  and  $\nu_{TT} = \nu_{NT} = \nu$  and Eq. (5) reduces to the classical result

$$K_D^{\text{I}} = \frac{E}{3(1 - 2\nu)} \quad (6)$$

117 The estimation of the skeletal bulk modulus of the Grimsel granite can be attempted provided that the elasticity  
118 constants applicable to either an isotropic fabric or a transversely isotropic skeletal elastic behaviour, can be identified.  
119 The geomechanical investigations of the granitic rocks at Grimsel have ranged from the estimation of the deformability  
120 and strength characteristics of the rock to the assessment of the in situ stress state. The interpretation of the available  
121 data for estimating the *skeletal deformability characteristics* is complicated by the fact that the approaches used are  
122 not uniform and standardized; the earlier experimental studies may have deviated from currently acceptable standards  
123 (as suggested by ASTM and ISRM) for sample size, rate of loading, end restraints, method of interpretation of  
124 the experimental data for parameter extraction (secant modulus, tangent modulus, loading/unloading paths, cycles),  
125 etc. The exercise is also compounded by the material variability in terms of the Grimsel lithology and its influence  
126 on parameter variability. Within these limitations, attempts can be made to extract, from the existing literature,  
127 representative values of the elasticity characteristics of Grimsel granite with due consideration for the species of  
128 granite. The earliest record used in this study relates to the work of Amiguet (1985) and Alonso and Alcoverro  
129 (2005), which indicate the elasticity properties as  $E \approx 60$  GPa;  $\nu \approx 0.25$ .

130 Pahl et al. (1989) used borehole dilatometer and overcoring to estimate the in-situ stress state and the overall  
131 deformability characteristics of the granite:  $E \approx 40$  GPa;  $\nu \approx 0.25$ . The work of Keusen et al. (1989) gives a range  
132 of elasticity values applicable to the granodiorite ( $\max[E \approx 63$  GPa;  $\nu \approx 0.48$ ];  $\min[E \approx 32$  GPa;  $\nu \approx 0.18$ ]) and  
133 the Aar granite ( $\max[E \approx 64$  GPa;  $\nu \approx 0.49$ ];  $\min[E \approx 42$  GPa;  $\nu \approx 0.25$ ]). Ziegler and Amann (2012) also report  
134 the results of an extensive series of tests conducted on both wet and dry and coarse-grained and fine-grained samples  
135 of Grimsel granite. The results are presented as maximum and minimum values as follows: for the coarse-grained  
136 granite,  $\max[E \approx 59$  GPa;  $\nu \approx 0.37$ ];  $\min[E \approx 53$  GPa;  $\nu \approx 0.25$ ]; for the medium-grained granite. The recent work  
137 of Bouffier (2015) uses laboratory over coring techniques to estimate the deformability characteristics of the Grimsel  
138 granite and there is a wide range of results for both the elastic modulus and Poisson's ratio; average representative  
139 results are indicated by  $E \approx 25$  GPa;  $\nu \approx 0.33$ . The work of Kant et al. (2017) is primarily focused on the estimation  
140 of the thermal properties of the Aar granite. The results they cite for the modulus of elasticity and Poisson's ratio are  
141 directly obtained from the work of Alonso et al. (2005) or indirectly from Keusen et al. (1989). Wenning et al. (2018)  
142 report studies of permeability and seismic velocity anisotropy across a ductile to brittle transition zone in the Grimsel  
143 granite.

144 The skeletal compressibility is also an important parameter in the interpretation of transient hydraulic pulse tests  
145 for estimating the fluid transport properties of low permeability materials including granite and argillaceous limestones  
146 (Brace et al., 1968; Selvadurai and Carnaffan, 1997; Selvadurai and Selvadurai, 2014; Selvadurai and Najari, 2015).  
147 The elasticity properties were determined via dynamic measurements and the maximum and minimum values are as  
148 follows:  $\max[E \approx 95$  GPa;  $\nu \approx 0.18$ ];  $\min[E \approx 65$  GPa;  $\nu \approx 0.15$ ]. Considering the nature of the ductile to brittle  
149 transmission zone under investigation and the dynamic nature of the tests, these estimates are far in excess of those  
150 for the intact material that is tested statically. Furthermore, the bulk modulus estimated from the maximum values of  
151  $E$  and  $\nu$  is in the range of 50 GPa, which is lower than the bulk modulus of mono-mineralic albite but exceeds that of



152 quartz. The study by Krietsch et al. (2019) deals with the characterization of the in situ stress state at the Grimsel test  
153 site, using a range of experiments including overcoring and hydraulic fracturing. The investigations were extended to  
154 include transverse isotropy of the rock mass.

155 The elasticity parameters were inferred through a computational back analysis of the overcoring technique; these  
156 authors also provide a comparison with the results obtained by Bouffier (2015). An averaging procedure gives maximum  
157 estimates of the isotropic elasticity parameters as  $E \approx 26$  GPa;  $\nu \approx 0.33$ . The use of the Grimsel Laboratory  
158 facility for the FEBEX experiment (Alonso and Alcoverro, 2005) provided a useful International Benchmarking exercise  
159 to validate THM modelling of clay buffer regions that could be used in high-level nuclear waste management  
160 endeavours. The international collaborative effort (Alonso et al., 2005) focused more on the behaviour of the clay barrier  
161 during heating from emplaced heaters and fluid influx from the Grimsel granite. In many of the research efforts  
162 for the FEBEX Project, the Grimsel granite served as a heat sink and the rock mechanics aspects perhaps received  
163 less emphasis (i.e. the modelling of the bentonitic clay under heating was considered to be the major objective of  
164 the research as opposed to the modelling of the Grimsel granite). Also, to enhance fluid influx, the Grimsel gallery  
165 was considered to be a fractured rock mass and modelling the Grimsel rock elasticity properties varied between the  
166 research groups participating in the FEBEX project, with very low estimates of the elasticity properties (Nguyen et al.,  
167 2005) to near intact rock properties derived from the original studies of Amiguet (1985) (see also Gens et al., 1998;  
168 Alonso and Alcoverro, 2005; Rutqvist et al., 2003; Dupray et al., 2013). For this reason, the elasticity properties of  
169 the Grimsel granite cited in the papers dealing with the FEBEX exercise are excluded from consideration.

170 The majority of the studies focusing on the evaluation of the deformability characteristics of the Grimsel granite  
171 deal with isotropic elastic modelling. The possible influences of either elastic anisotropy or elastic transverse isotropy  
172 were addressed in the earlier study by Pahl et al. (1989) in connection with the estimation of in situ stress states. In  
173 this particular study, there is no clear statement of the applicable value of the elasticity constants governing transverse  
174 isotropy of the Grimsel granite (the degree of anisotropy ( $E_T/E_N$ ) does not exceed 1.25) and the study culminates  
175 in the adoption of the isotropic elasticity properties that were indicated previously. The research by Nejati (2018)  
176 and Nejati et al. (2019) deals with the estimation of the deformability characteristics of the Grimsel granite based  
177 on the transversely isotropic elastic model with principal directions aligned in the stratification planes and normal to  
178 the planes (Figure 2). These studies indicate that the Grimsel granite tested also exhibited significant anisotropy and  
179 nonlinearity. In addition, due to nonlinear effects, the secant, tangent and average values of the Young's modulus can  
180 depend on the stress level at which the value is estimated.

181 If a range of elastic behaviour can be clearly defined and if the elastic constants governing transverse isotropy can  
182 be determined, then, as shown by Eq. (5), the bulk modulus applicable to the transversely isotropic material can be  
183 evaluated objectively. The studies conducted by Nejati (2018) and Nejati et al. (2019) provide the following estimates  
184 for the elastic constants governing the transversely isotropic elasticity model for the Grimsel granite:  $E_N \approx 30$  GPa;  
185  $E_T \approx 47$  GPa;  $\nu_{TT} \approx 0.20$  GPa;  $\nu_{NT} \approx 0.10$  GPa. Finally, Krietsch et al. (2019) conducted a series of experiments on  
186 the ISC core plugs, using overcoring and external pressurization of the hollow samples. These authors also give results  
187 of uniaxial tests conducted on core plugs extracted either normal or parallel to the foliations (Figure 18 of their paper).  
188 These results can be used to estimate the  $E_N$  and  $E_T$ . From the results presented by Krietsch et al. (2019), the relevant  
189 elastic moduli can be summarized as follows:  $E_N \approx 13$  GPa;  $E_T \approx 35$  GPa. These investigations, however, cannot be  
190 used to estimate the values of  $\nu_{TT}$  and  $\nu_{NT}$ . Dambly et al. (2019) presented the results of a research program geared to  
191 estimate the transversely isotropic elasticity parameters from results of ultrasonic dynamic tests and static tests. Nejati  
192 et al. (2019) compared the static and dynamic values of the elastic constants at zero-confinement, and concluded that





193 the dynamic moduli are significantly greater than the static ones. In this study we have not considered experimental  
 194 results derived from dynamic testing; therefore, for consistency, any results derived from dynamic testing of the  
 195 Grimsel granite have been excluded from further consideration. Considering the experimental evaluations available  
 196 in the literature, the elasticity parameters applicable to the Grimsel granite are summarized in Table 5.

Table 5: Elasticity Properties for the Grimsel Granite with the corresponding  $K_D^I$  or  $K_D^{II}$  values:  $K_D^I = E/3(1 - 2\nu)$ ,  $K_D^{II} = E_T E_N / [2E_N(1 - \nu_{TT}) + E_T(1 - 4\nu_{NT})]$ ;  $N$  signifies the direction normal to the planes of stratification and  $T$  signifies the directions along the planes of stratification.

Reference	Elasticity Type	Elastic Constants	$K_D^I$ or $K_D^{II}$
Amiguet (1985) <sup>1</sup>	Isotropic	$E = 60$ GPa; $\nu = 0.25$	$K_D^I \approx 40$ GPa
Pahl et al. (1989)	Isotropic	$E = 40$ GPa; $\nu = 0.25$	$K_D^I \approx 27$ GPa
Keusen et al. (1989) (Granodiorite)	Isotropic	mean $E \approx 47$ GPa; $\nu \approx 0.33$	$(K_D^I)_{\text{mean}} \approx 46$ GPa
Keusen et al. (1989) (Aar granite)	Isotropic	mean $E \approx 53$ GPa; $\nu \approx 0.37$	$(K_D^I)_{\text{mean}} \approx 68$ GPa
Ziegler and Amann (2012) Type 1–coarse grained	Isotropic	mean $E \approx 38$ GPa; $\nu \approx 0.36$	$(K_D^I)_{\text{mean}} \approx 45$ GPa
Ziegler and Amann (2012) Type 2–medium grained	Isotropic	mean $E \approx 43$ GPa; $\nu \approx 0.37$	$(K_D^I)_{\text{mean}} \approx 55$ GPa
Bouffier (2015)	Isotropic	$E = 26$ GPa; $\nu = 0.33$	$K_D^I \approx 25$ GPa
Dambly et al. (2019) <sup>1</sup>	Isotropic	$E = 44$ GPa; $\nu = 0.2$	$K_D^I \approx 24$ GPa
Krietsch et al. (2019) <sup>2</sup>	Transversely Isotropic	$E_N \approx 13$ GPa; $E_T \approx 35$ GPa; $\nu_{TT} \approx 0.15$ ; $\nu_{NT} \approx 0.15$	$K_D^{II} \approx 13$ GPa
Nejati et al. (2019); Nejati (2018) <sup>3</sup>	Transversely Isotropic	$E_N \approx 30$ GPa; $E_T \approx 47$ GPa; $\nu_{TT} \approx 0.2$ ; $\nu_{NT} \approx 0.1$	$K_D^{II} \approx 19$ GPa

### 197 3. Compressibility of the Solid Material Composing the Grimsel Granite Fabric

198 The skeletal material of the Grimsel granite consists of a variety of mineral phases including quartz, biotite,  
 199 anorthite, augite, microcline and traces of pyrite and magnetite. The composition of these minerals were determined  
 200 both at the XRD facilities at University of Montréal, QC, Canada and at the Department of Earth Sciences, Institute  
 201 of Geology, ETH, Zurich (Wenning et al., 2018). The estimated volume fractions and the values for the bulk moduli  
 202 and shear moduli are shown in Tables 6 and 7 respectively. The average volume fractions and the mineralogical  
 203 compositions tend to vary and the estimated values are, in general, considered to be approximate. The results of the  
 204 XRD evaluations do not provide sufficient accuracy to group the tested rocks into either the Grimsel granodiorite or  
 205 the FEBEX Grimsel categories. A very cursory comparison with the data provided in Tables 1 to 3 would suggest  
 206 that the mineralogical compositions provided by Wenning et al. (2018) and indicated in Table 6 correspond to the  
 207 Grimsel granodiorite and the results shown in Table 7 correspond to the FEBEX granite. For this reason, the XRD  
 208 data derived from both laboratory evaluations (ETH and McGill) are retained in the estimations of the solid material  
 209 compressibility  $K_S$ . Also, the void fraction ( $\ll 1\%$ ) is neglected in the calculations. The values for the bulk moduli  
 210 and shear moduli for the various minerals were obtained from published literature (Alexandrov et al., 1964; Anderson  
 211 and Nafe, 1965; Carmichael, 1990; Sisodia and Verma, 1990; Moos et al., 1997; Redfern and Angel, 1999; Schilling  
 212 et al., 2003; Zhu et al., 2007; Mavko et al., 2009; Lin, 2013).

213 In the multi-phasic approach, the objective is to determine the overall bulk modulus for the solid mineralogical  
 214 phase by considering the bulk moduli for the separate mineral constituents and their volume fractions. Ideally this

<sup>1</sup>This estimate is based on the elastic constants measured along the foliations.

<sup>2</sup>This estimate is based on the secant elastic constants at a stress level of approximately 9 MPa.

<sup>3</sup>This estimate is based on tangent elastic constants at the in-situ stress level based on the analyses of Krietsch et al. (2019), which is approximately 11 MPa.



Table 6: Mineralogical Fractions of the Grimsel Granite [Data obtained by Wenning et al. (2018), Institute of Geology, ETH, Zurich].

Mineral	Specific Gravity	%	$K_S$ (GPa)	$G_S$ (GPa)
<b>Biotite &amp; Phlogopite</b>	2.72	10	77	42
<b>Muscovite</b>	2.70	5	61	41
<b>Epidote</b>	2.75	6	107	60
<b>Albite</b>	3.19	40	76	26
<b>Feldspar</b>	2.60	16	76	26
<b>Quartz</b>	2.72	23	38	45
		$\Sigma$ 100		

Table 7: Mineralogical Fractions of the Grimsel Granite [Data obtained by the Earth Sciences Laboratory, University of Montréal].

Mineral	Specific Gravity	%	$K_S$ (GPa)	$G_S$ (GPa)
<b>Quartz</b>	2.72	46	38	45
<b>Biotite</b>	2.70	5	77	42
<b>Anorthite</b>	2.75	37	68	38
<b>Augite</b>	3.19	5	95	59
<b>Microcline</b>	2.60	7	52	36
		$\Sigma$ 100		

215 needs to be approached using a generalized theory of multi-phasic composites that can accommodate a mixture of any  
 216 number of phases. Such a generalized theory is yet to be developed. The most widely used relationships are those by  
 217 Voigt (1928) and Reuss (1929). The Voigt ( $^V$ ) and the Reuss ( $^R$ ) estimates are

$$\begin{aligned}
 (K_S)_I^V &= \sum_i^n V_i (K_S)_i, & (K_S)_I^R &= \left[ \sum_i^n \frac{V_i}{(K_S)_i} \right]^{-1} \\
 (G_S)_I^V &= \sum_i^n V_i (G_S)_i, & (G_S)_I^R &= \left[ \sum_i^n \frac{V_i}{(G_S)_i} \right]^{-1}
 \end{aligned} \quad (7)$$

$i = \text{Qtz, Biotite, Anorthite, Augite, Microcline, Voids}$   
 $I = \text{Data from Table 1 or Table 2}$

218 The results given in Hill (1952, 1965) are the mean of the Voigt and Reuss estimates. This basic approach can be  
 219 applied to estimate the effective bulk and shear moduli for the Grimsel granite: i.e.

$$(K_S)_I = \frac{1}{2} \left[ (K_S)_I^V + (K_S)_I^R \right], \quad (G_S)_I = \frac{1}{2} \left[ (G_S)_I^V + (G_S)_I^R \right] \quad (8)$$

$I = \text{Data from Table 1 or Table 2}$

220 Using the mineralogical compositions obtained from XRD analyses given in Table 1, we have

$$(K_S)_1 = 65 \text{ GPa}, \quad (G_S)_1 = 33 \text{ GPa} \quad (9)$$

221 and using the mineralogical compositions obtained from XRD analyses given in Table 2, we have

$$(K_S)_2 = 52 \text{ GPa}, \quad (G_S)_2 = 48 \text{ GPa} \quad (10)$$

222 A further approach is to use the Voigt and Reuss estimates for  $(K_S)_I$  and  $(G_S)_I$ , ( $I = 1, 2$ ) in the Hashin and  
 223 Shtrikman (1963) results to develop bounds for the compressibility of the solid constituents of the Grimsel granite.  
 224 The Hashin-Shtrikman results in conjunction with the Voigt and Reuss estimates can be evaluated to estimate the upper  
 225 and lower bounds  $(K_S)_I^U$  and  $(K_S)_I^L$ , ( $I = 1, 2$ ) for the compressibility of the solid material of the Grimsel granite.



226 Assuming that a fraction  $\phi$  of the Grimsel granite will satisfy the Voigt estimate (or the Reuss estimate), the lower  
 227  $(K_S)^L$  and upper  $(K_S)^U$  Hashin-Shtrikman bounds for the compressibility of the solid phase, represented by  $(K_S)^L$  and  
 228  $(K_S)^U$ , can be obtained from the results

$$(K_S)_I^L = (K_S)_I^V + \frac{\phi}{\frac{1}{(K_S)_I^R - (K_S)_I^V} + \left(\frac{3(1-\phi)}{3(K_S)_I^V + 4(G_S)_I^V}\right)}, \quad (I = 1, 2) \quad (11)$$

229 and

$$(K_S)_I^U = (K_S)_I^R + \frac{1-\phi}{\frac{1}{(K_S)_I^V - (K_S)_I^R} + \left(\frac{3\phi}{3(K_S)_I^R + 4(G_S)_I^R}\right)}, \quad (I = 1, 2) \quad (12)$$

230 These bounds converge to the proper limits as  $\phi \rightarrow 1$  and  $\phi \rightarrow 0$ . The unknown in Eqs. (11) and (12) relates to  
 231 the volume fraction  $\phi$  that will be relevant to the partitioning of fractions of the multi-phasic system that will obey the  
 232 Voigt and Reuss estimates. There is no physical principle that can be adopted to determine this partitioning, *a priori*.  
 233 In order to provide a comparison to the Voigt-Reuss-Hill estimate, we can evaluate the expressions (11) and (12) for  
 234  $\phi = 1/2$ , since the Hill estimate is the mean of the Voigt and Reuss estimates. The results for the Hashin-Rosen  
 235 estimates derived from (11) and (12) give

$$(K_S)_1^L \approx 54.4 \text{ GPa}, \quad (K_S)_2^L \approx 68.5 \text{ GPa} \quad (13)$$

236 and

$$(K_S)_1^U \approx 49.6 \text{ GPa}, \quad (K_S)_2^U \approx 62.1 \text{ GPa} \quad (14)$$

237 Considering the limits of the Hashin-Shtrikman estimates for the upper and lower bounds for the solid material  
 238 compressibility of the Grimsel granite, the *average estimates* for the solid material compressibilities obtained from  
 239 the two sets of laboratory data give

$$(K_S)_1 \in (49.6, 54.4) \text{ GPa}, \quad (K_S)_2 \in (62.1, 68.5) \text{ GPa} \quad (15)$$

240 Considering the range of solid material compressibilities obtained from the two laboratory investigations we can  
 241 conclude that the lower ( $^L$ ) and upper ( $^U$ ) estimates for  $K_S$  are approximately

$$K_S^L \approx 50 \text{ GPa}, \quad K_S^U \approx 69 \text{ GPa} \quad (16)$$

242 The results for the skeltal compressibilities given in Table 5 can be combined with the range of solid material  
 243 compressibilities to estimate the *upper* and *lower* limits of the Biot coefficient applicable to each estimate of  $K_D^I$  and  
 244  $K_D^{II}$ . The relevant results are shown in Table 8.

#### 245 4. Discussion

246 In theories developed for estimating the elasticity of multi-phasic materials, the most extensive studies relate to  
 247 two-component elastic materials. Theories, however, have also been developed by several researchers to include a



Table 8: Upper and lower limits for the Biot coefficient for the Grimsel Granite;  $\alpha_U = 1 - (K_D^I \text{ or } K_D^{II})/K_S^U$ ,  $\alpha_L = 1 - (K_D^I \text{ or } K_D^{II})/K_S^L$ ,  $K_S^L \approx 50$  GPa,  $K_S^U \approx 69$  GPa.

Reference	Elasticity Type	$K_D^I$ or $K_D^{II}$	$\alpha_L$	$\alpha_U$
Amiguet (1985)	Isotropic	$K_D^I \approx 40$ GPa	0.19	0.42
Pahl et al. (1989)	Isotropic	$K_D^I \approx 27$ GPa	0.46	0.61
Keusen et al. (1989) (Granodiorite)	Isotropic	$(K_D^I)_{mean} \approx 46$ GPa	0.07	0.33
Keusen et al. (1989) (Aar granite)	Isotropic	$(K_D^I)_{mean} \approx 68$ GPa	-0.37	0.01
Ziegler and Amann (2012) Type 1-coarse grained	Isotropic	$(K_D^I)_{mean} \approx 45$ GPa	0.09	0.34
Ziegler and Amann (2012) Type 2-medium grained	Isotropic	$(K_D^I)_{mean} \approx 55$ GPa	-0.10	0.20
Bouffier (2015)	Isotropic	$K_D^I \approx 25$ GPa	0.50	0.64
Dambly et al. (2019)	Isotropic	$K_D^I \approx 24$ GPa	0.52	0.65
Krietsch et al. (2019)	Transversely Isotropic	$K_D^{II} \approx 13$ GPa	0.74	0.81
Nejati et al. (2019); Nejati (2018)	Transversely Isotropic	$K_D^{II} \approx 19$ GPa	0.62	0.72

248 distribution of three elastic phases in the composite material. An early study in this area is by Cohen and Ishai (1967)  
 249 that considered the presence of a large voids content in the two-phase system. Several other developments have been  
 250 proposed in the literature; references to such studies are given by Ju and Chen (1994a,b) and the references cited in  
 251 the introduction. The extension to three elastic phases was also presented in the studies by Talbot et al. (1995) and,  
 252 more recently, by Lin and Ju (2009). Even with these developments, the number of separate components included in  
 253 the composite material models are insufficient to accommodate all the components of the solid phases listed in Tables  
 254 1 to 3 and 5 and 6.

255 A plausible alternate approach is to essentially reduce the components in Tables 1 and 2 to three phases by com-  
 256 bining (using the Voigt-Reuss-Hill approach) the material phases that correlate closely in terms of their bulk and shear  
 257 moduli values. Whether, in view of the approximate nature of the XRD evaluations of the volume fractions of the  
 258 separate phases, such refinements are altogether warranted is debatable. The results of the evaluations presented in the  
 259 paper suggest that the multi-phasic approach in conjunction with XRD data provides a useful alternative to validating  
 260 the conventional experimental approach for estimating the solid material composing low permeability porous media.  
 261 The skeletal bulk moduli for the Grimsel granite shows a wide variation, indicative of variable lithology of the igneous  
 262 rock formation. In this sense it is prudent to assume a set of limits for the choice of the Biot coefficient rather than  
 263 to assign a specific value. Certain data obtained in this study give rise to non-realistic values of the Biot coefficient,  
 264 clearly arising from the estimation of the skeletal compressibility.

265 As a guide, experimental results for the skeletal compressibility values that exceed the effective solid material  
 266 compressibility of the minerals with the largest volume fractions should be disregarded. Therefore these results can  
 267 be excluded without further comment. (i.e. Since the multi-phasic assessment of the compressibility of the solid  
 268 material has a lower limit of approximately  $K_S^L \approx 50$  GPa, plausible values of the Biot coefficient will be obtained  
 269 when  $K_D < K_S^L$ .) Also, excessively low values of  $K_D$  need to be re-examined before using the data to estimate the  
 270 Biot coefficient. Excessively low values can result from inaccurate estimation of the elastic modulus and Poisson's  
 271 ratio. Similarly, excessively high values of the skeletal stiffness can result from inaccurate estimates of the Poisson's  
 272 ratio of the rock. For example, if samples are loaded in the direction of the foliations or stratifications, micro-crack  
 273 or defect development during compression can give rise to lateral deformations that can be a result of void/crack  
 274 generation and not a result of material deformation. Considering the numerical values presented in Table 8, and the  
 275 above comments, several estimates for the Biot coefficients can be excluded from further discussion. The Table 9  
 276 summarizes the revised set of realistic experimental estimates for the Biot coefficient of the Grimsel granite, taking



277 into consideration the aforementioned caveats on the experimental results.

Table 9: Reduced Data Set for the Upper and Lower Limits for the Biot coefficient for the Grimsel Granite.

Reference	Elasticity Type	$K_D^I$ or $K_D^{II}$	$\alpha_L$	$\alpha_U$
Pahl et al. (1989)	Isotropic	$K_D^I \approx 27$ GPa	0.46	0.61
Bouffier (2015)	Isotropic	$K_D^I \approx 25$ GPa	0.50	0.64
Dambly et al. (2019)	Isotropic	$K_D^I \approx 24$ GPa	0.52	0.65
Nejati et al. (2019); Nejati (2018)	Transversely Isotropic	$K_D^{II} \approx 19$ GPa	0.62	0.72

## 278 5. Conclusions

279 The accurate estimation of the skeletal deformability characteristics of a porous rock is an essential pre-requisite  
280 for estimating the Biot coefficient for a fluid-saturated poroelastic material. While the procedures for conducting either  
281 uniaxial or triaxial tests to estimate the skeletal deformability characteristics are well known, the exact procedure  
282 for estimating the elastic moduli, Poisson's ratio, etc., needs to be better documented so that the interpretations of  
283 experimental data can be consistent. The conventional procedure for the pressurization of a saturated sample of  
284 the rock and the measurement of the resulting sample strains when the externally applied cell pressure matches the  
285 pore fluid pressure is perhaps the best procedure for estimating the compressibility of the solid phases of the porous  
286 medium. This, however, is not a routine procedure for low permeability materials and substantial pressures need to be  
287 applied to ensure that volumetric strains of an accurately measurable value can be recorded.

288 Also, in such cases the strains could involve irreversible grain boundary frictional slip and this needs to be excluded  
289 from the estimation of the solid material compressibility. Here, we advocate the use of a multi-phasic approach where  
290 the theories of composite materials can be used to estimate the compressibility of the solid material composing the  
291 porous skeleton. This is a relatively easy approach since XRD evaluations of the mineralogical phase composition are  
292 usually carried out to characterize the rock. In relation to the Grimsel granite, the analysis points to a Biot coefficient  
293 that has bounds rather than a specific value: i.e.  $0.46 < \alpha < 0.72$ . Values for the Biot coefficient for other types of  
294 rocks include [see also Table 1 in Detournay and Cheng (1993)]: Westerly granite ( $\alpha \approx 0.47$ ); for the Lac du Bonnet  
295 granite in Manitoba, Canada, a value of  $\alpha = 0.73$  is cited (Lau and Chandler, 2004); Ruhr sandstone ( $\alpha \approx 0.65$ );  
296 Berea sandstone ( $\alpha \approx 0.79$ ); Weber sandstone ( $\alpha \approx 0.64$ ); Ohio sandstone ( $\alpha \approx 0.65$ ); Pecos sandstone ( $\alpha \approx 0.83$ );  
297 Boise sandstone ( $\alpha \approx 0.85$ ); Cobourg limestone ( $\alpha \approx 0.66$ ). With soft rocks such as chalk, the Biot coefficient is  
298 invariably in the range 0.80 to 1.0 (Alam et al., 2010; Nermoen et al., 2013). For the Callovo-Oxfordian claystone the  
299 Biot coefficient is estimated to be in the range of 0.84 (Belmokhtar et al., 2018). Other estimates for a variety of rocks  
300 encountered in a coal mining setting are also given by Chen et al. (2019).

## 301 Acknowledgement

302 The work described in the paper was supported by a Discovery Research Grant awarded by the Natural Sciences  
303 and Engineering Research Council of Canada. This study is part of the In situ Stimulation and Circulation (ISC)  
304 project established by the Swiss Competence Center for Energy Research-Supply of Electricity (SCCER-SoE) with  
305 the support of Innosuisse. The authors are also grateful to Professor Eduardo Alonso (UPC, Spain), Professor Lyesse  
306 Laloui (EPFL, Switzerland), Professor Florian Amman (RWTH, Germany), Professor Martin Mazurek (University  
307 of Bern, Switzerland), Dr. Stratis Vomvoris (NAGRA, Switzerland), Professor Christian David (Université Cergy-  
308 Pontoise, France), Dr. Jonny Rutqvist (LBNL, USA), Dr. Farid Laouafa (INERIS, France) and Dr. Son Nguyen



309 (CNSC, Canada) for drawing attention to the literature used in this study and for helpful comments. The authors  
310 gratefully acknowledge the comments made by Dr. Joseph Doetsch, Institute of Geophysics, Department of Earth  
311 Sciences ETH Zurich, which led to improvements in the presentation. The authors, however, are entirely responsible  
312 for the statements and conclusions presented in the paper.

### 313 References

- 314 Alam, M. M., Borre, M. K., Fabricius, I. L., Hedegaard, K., Røgen, B., Hossain, Z., Krogsbøll, A. S., 2010. Biot's coefficient as an indicator  
315 of strength and porosity reduction: Calcareous sediments from Kerguelen Plateau. *Journal of Petroleum Science and Engineering* 70 (3-4),  
316 282–297.
- 317 Alexandrov, K. S., Rhyzova, T. V., Beliko, B. P., 1964. The elastic properties of pyroxenes. *Soviet Physics-Crystallography* 8, 589–591.
- 318 Alonso, E. E., Alcoverro, J., 2005. DECOVALEX III PROJECT. Modelling of FEBEX In-Situ Test, Task 1 Final Report. Tech. rep., SKI Report  
319 2005:20.
- 320 Alonso, E. E., Alcoverro, J., Coste, F., Malinsky, L., Merrien-Soukatchoff, V., Kadiri, I., Nowak, T., Shao, H., Nguyen, T. S., Selvadurai, A. P. S.,  
321 Armand, G., Sobolik, S. R., Itamura, M., Stone, C. M., Webb, S. W., Rejeb, A., Tijani, M., Maouche, Z., Kobayashi, A., Kurikami, H., Ito, A.,  
322 Sugita, Y., Chijimatsu, M., Börgesson, L., Hernelind, J., Rutqvist, J., Tsang, C. F., Jussila, P., 2005. The FEBEX benchmark test: Case definition  
323 and comparison of modelling approaches. *International Journal of Rock Mechanics and Mining Sciences* 42, 611–638.
- 324 Amann, F., Gischig, V., Evans, K., Doetsch, J., Jalali, R., Valley, B., Krietsch, H., Dutler, N., Villiger, L., Brixel, B., Klepikova, M., Kittilä, A.,  
325 Madonna, C., Wiemer, S., Saar, M. O., Loew, S., Driesner, T., Maurer, H., Giardini, D., 2018. The seismo-hydromechanical behavior during  
326 deep geothermal reservoir stimulations: open questions tackled in a decameter-scale in situ stimulation experiment. *Solid Earth* 9 (1), 115–137.
- 327 Amiguet, J.-L., 1985. Grimsel Test Site. Felskennwerte von intaktem Granit. Zusammenstellung felsmechanischer Laborresultate diverser granit-  
328 scher Gesteine. Tech. rep., NAGRA, NIB 85-08.
- 329 Anderson, O. L., Nafe, J. E., 1965. The bulk modulus-volume relationship for oxide compounds and related geophysical problems. *Journal of*  
330 *Geophysical Research* 70 (16), 3951–3963.
- 331 Belmokhtar, M., Delage, P., Ghabezloo, S., Conil, N., 2018. Drained Triaxial Tests in Low-Permeability Shales: Application to the Callovo-  
332 Oxfordian Claystone. *Rock Mechanics and Rock Engineering* 51 (7), 1979–1993.
- 333 Biot, M. A., 1941. General theory of three-dimensional consolidation. *Journal of Applied Physics* 12 (2), 155–164.
- 334 Bouffier, C., 2015. Stress measurements by overcoring at the Grimsel site. Results from the campaign of August-September 2015 Study Report.  
335 Tech. rep., ETH Zurich, <https://doi.org/10.3929/ethz-b-000256660>.
- 336 Brace, W., Walsh, J., Frangos, W., 1968. Permeability of Granite under High Pressure. *Journal of Geophysical Research* 73 (6), 2225–2236.
- 337 Carmichael, R. S., 1990. *Practical Handbook of Physical Properties of Rocks and Minerals*. CRC Press, Boca Raton, FL.
- 338 Chen, Y., Selvadurai, A. P. S., Liang, W., 2019. Computational Modelling of Groundwater Inflow During a Longwall Coal Mining Advance: A  
339 Case Study from the Shanxi Province, China. *Rock Mechanics and Rock Engineering* 52 (3), 917–934.
- 340 Cheng, A. H. D., 2015. *Poroelasticity*. Springer-Verlag, Berlin.
- 341 Cohen, L., Ishai, O., 1967. The elastic properties of three-phase composites. *Journal of Composite Materials* 1, 390–403.
- 342 Dambly, M., Nejati, M., Vogler, D., Saar, M. O., 2019. On the direct measurement of the shear moduli in transversely isotropic rocks using the  
343 uniaxial compression test. *International Journal of Rock Mechanics and Mining Sciences* 113, 220–240.
- 344 David, C., Wassermann, J., Amann, F., Klaver, J., Davy, C., Sarout, J., Esteban, L., Rutter, E. H., Hu, Q., Louis, L., Delage, P., Lockner, D. A.,  
345 Selvadurai, A. P. S., Vanorio, T., Hildenbrand, A. A., Meredith, P. G., Browning, J., Mitchell, T. M., Madonna, C., Billiotte, J., Reuschlé, T.,  
346 Lasseux, D., Fortin, J., Lenormand, R., Loggia, D., Nono, F., Boitnott, G., Jahns, E., Fleury, M., Berthe, G., Braun, P., Grégoire, D., Perrier,  
347 L., Polito, P., Jannot, Y., Sommier, A., Krooss, B., Fink, R., Clark, A., 2018a. KG2B, a collaborative benchmarking exercise for estimating  
348 the permeability of the Grimsel granodiorite-Part 2: Modelling, microstructures and complementary data. *Geophysical Journal International*  
349 215 (2), 825–843.
- 350 David, C., Wassermann, J., Amann, F., Lockner, D. A., Rutter, E. H., Vanorio, T., Hildenbrand, A. A., Billiotte, J., Reuschlé, T., Lasseux, D., Fortin,  
351 J., Lenormand, R., Selvadurai, A. P. S., Meredith, P. G., Browning, J., Mitchell, T. M., Loggia, D., Nono, F., Sarout, J., Esteban, L., Davy, C.,  
352 Louis, L., Boitnott, G., Madonna, C., Jahns, E., Fleury, M., Berthe, G., Delage, P., Braun, P., Grégoire, D., Perrier, L., Polito, P., Jannot,  
353 Y., Sommier, A., Krooss, B., Fink, R., Hu, Q., Klaver, J., Clark, A., 2018b. KG2B, a collaborative benchmarking exercise for estimating the  
354 permeability of the Grimsel granodiorite - Part 1: Measurements, pressure dependence and pore-fluid effects. *Geophysical Journal International*  
355 215 (2), 799–824.
- 356 Davis, R. O., Selvadurai, A. P. S., 1996. *Elasticity and Geomechanics*. Cambridge University Press, Cambridge.



- 357 Detournay, E., Cheng, A. H. D., 1993. Comprehensive rock engineering: Principles, practice and projects. In: Hudson JA, ed., Fundamentals of  
358 Poroelasticity, vol. 1. Pergamon Press, Oxford.
- 359 Doetsch, J., Gischig, V., Villiger, L., Krietsch, H., Nejati, M., Amann, F., Jalali, M., Madonna, C., Maurer, H., Wiemer, S., Driesner, T., Giardini, D.,  
360 2018. Subsurface fluid pressure and rock deformation monitoring using seismic velocity observations. *Geophysical Research Letters*, Accepted  
361 for publication.
- 362 Dupray, F., François, B., Laloui, L., 2013. Analysis of the FEBEX multi-barrier system including thermoplasticity of unsaturated bentonite.  
363 *International Journal for Numerical and Analytical Methods in Geomechanics* 37, 399–422.
- 364 Dutler, N., Nejati, M., Valley, B., Amann, F., Molinari, G., 2018. On the link between fracture toughness, tensile strength, and fracture process  
365 zone in anisotropic rocks. *Engineering Fracture Mechanics* 201, 56–79.
- 366 Francfort, G. A., Murat, F., 1986. Homogenization and optimal bounds in linear elasticity. *Archive for Rational Mechanics and Analysis* 94 (4),  
367 307–334.
- 368 Garralón, A., Gómez, P., Turrero, M. J., Torres, E., Buil, B., Pea, J., 2017. Hydrogeochemical characterization of the groundwater in the FEBEX  
369 gallery, National Cooperative for the Disposal of Radioactive Waste. Tech. rep., NAGRA Arbeitsbericht, NAB 16-14, Wettingen, Switzerland.
- 370 Gens, A., Garcia-Molina, A. J., Olivella, S., Alonso, E. E., Huertas, F., 1998. Analysis of a full scale in situ testing simulating repository conditions.  
371 *International Journal for Numerical and Analytical Methods in Geomechanics* 22 (7), 515–548.
- 372 Gischig, V. S., Doetsch, J., Maurer, H., Krietsch, H., Amann, F., Frederick Evans, K., Nejati, M., Jalali, M., Valley, B., Christine Obermann, A.,  
373 Wiemer, S., Giardini, D., 2018. On the link between stress field and small-scale hydraulic fracture growth in anisotropic rock derived from  
374 microseismicity. *Solid Earth* 9 (1), 39–61.
- 375 Goncalves, P., Oliot, E., Marquer, D., Connolly, J. A., 2012. Role of chemical processes on shear zone formation: An example from the grimsel  
376 metagranodiorite (Aar massif, Central Alps). *Journal of Metamorphic Geology* 30 (7), 703–722.
- 377 Hashin, Z., Shtrikman, S., 1963. A variational approach to the theory of the elastic behaviour of multiphase materials. *Journal of the Mechanics*  
378 *and Physics of Solids* 11 (42), 127–140.
- 379 Hearmon, R. F. S., 1961. *An Introduction to Applied Anisotropic Elasticity*. Clarendon Press, Oxford.
- 380 Hill, R., 1952. The elastic behaviour of a crystalline aggregate. *Proceedings of the Physical Society A* 65, 349–354.
- 381 Hill, R. R., 1965. A self-consistent mechanics of composite materials. *Journal of the Mechanics and Physics of Solids* 13, 213–222.
- 382 Jalali, M., Gischig, V., Doetsch, J., Naf, R., Krietsch, H., Klepikova, M., Amann, F., Giardini, D., 2018. Transmissivity changes and microseismicity  
383 induced by smallscale hydraulic fracturing tests in crystalline rock. *Geophysical Research Letters* 45, 2265–2273.
- 384 Jokelainen, L., Meski, T., Lindberg, A., Soler, J. M., Siitari-Kauppi, M., Martin, A., Eikenberg, J., 2013. The determination of <sup>134</sup>Cs and <sup>22</sup>Na  
385 diffusion profiles in granodiorite using gamma spectroscopy. *Journal of Radioanalytical and Nuclear Chemistry* 295 (3), 2153–2161.
- 386 Ju, J. W., Chen, T. M., 1994a. Effective elastic moduli of two-phase composites containing randomly dispersed spherical inhomogeneities. *Acta*  
387 *Mechanica* 103 (1-4), 123–144.
- 388 Ju, J. W., Chen, T. M., 1994b. Micromechanics and effective moduli of elastic composites containing randomly dispersed ellipsoidal inhomog-  
389 eneities. *Acta Mechanica* 103 (1-4), 103–121.
- 390 Kant, M. A., Ammann, J., Rossi, E., Madonna, C., Höser, D., Rudolf von Rohr, P., 2017. Thermal properties of Central Aare granite for temperatures  
391 up to 500C: Irreversible changes due to thermal crack formation. *Geophysical Research Letters* 44 (2), 771–776.
- 392 Keusen, H., Ganguin, J., Schuler, P., Buletli, M., 1989. Technical report 87-14 E: Grimsel test site geology. Tech. rep., GEOTEST: Zollikofen /  
393 Bern.
- 394 Krietsch, H., Gischig, V., Evans, K., Doetsch, J., Dutler, N. O., Valley, B., Amann, F., 2019. Stress Measurements for an In Situ Stimulation Ex-  
395 periment in Crystalline Rock: Integration of Induced Seismicity, Stress Relief and Hydraulic Methods. *Rock Mechanics and Rock Engineering*  
396 52 (2), 517–542.
- 397 Lau, J. S. O., Chandler, N. A., 2004. Innovative laboratory testing. *International Journal of Rock Mechanics and Mining Sciences* 41, 1427–1445.
- 398 Lekhnitskii, S. G., 1963. *Theory of Elasticity of an Anisotropic Elastic Body*. Holden-Day, San Francisco.
- 399 Lin, C. C., 2013. Elasticity of calcite: Thermal evolution. *Physics and Chemistry of Minerals* 40 (2), 157–166.
- 400 Lin, P. J., Ju, J. W., 2009. Effective elastic moduli of three-phase composites with randomly located and interacting spherical particles of distinct  
401 properties. *Acta Mechanica* 208 (1-2), 11–26.
- 402 Mavko, G. M., Dvorkin, J., Mukerji, T., 2009. *The Rock Physics Handbook, Tools for seismic analysis of porous media*. Cambridge University  
403 Press, Cambridge.
- 404 Missana, T., Garcia-Gutiérrez, M., 2012. Comparison of the Cesium adsorption on different crystalline rocks, in 1st Workshop Proceedings of the  
405 Collaborative Project Crystalline Rock Retention Processes, (7th EC FP CP CROCK) (Rabung, T., Molinero, J., Garcia, D., Montoya, V., Eds).  
406 KIT Scientific Publishing, Barcelona, Spain.
- 407 Moos, D., Dvorkin, J., Hooks, A. J., 1997. Application of theoretically derived rock physics relationships  $\epsilon$  Los Angeles "Critical porosity".  
408 *Geophysical Research Letters* 24 (3), 329–332.



- 409 Möri, A., Mazurek, M., Adler, M., Schild, M., Siegesmund, S., Vollbrecht, A., Ota, K., Ando, T., Alexander, R., Smith, P. A., Haag, P. C., B., 2003.  
410 The Nagra-JNC in situ study of safety relevant radionuclide retardation in fractured crystalline rock. IV: The in situ study of matrix porosity in  
411 the vicinity of a water conducting fracture. Tech. rep., NAGRA Technical Report, 00-08, Baden, Switzerland.
- 412 Moulu, J. C., Kalaydjian, F., Tsakiroglou, C. D., Burganos, V. N., Payatakes, A. C., Yao, J., Thovert, J.-F., Adler, P.-M., 1997. Characterization,  
413 reconstruction and transport properties of the Vosges sandstone. *Revue de L'Institut Francais du Petrole* 52, 3–21.
- 414 Nejati, M., 2018. On the anisotropy of mechanical properties in Grimsel granodiorite. Tech. rep., ETH Zurich, [https://doi.org/10.3929/ethz-b-](https://doi.org/10.3929/ethz-b-000289969)  
415 [000289969](https://doi.org/10.3929/ethz-b-000289969).
- 416 Nejati, M., Dambly, M., , Saar, M. O., 2019. A methodology to determine the elastic properties of anisotropic rocks from a single uniaxial  
417 compression test. *Journal of Rock Mechanics and Geotechnical Engineering*, Accepted for publication.
- 418 Nermoen, A., Korsnes, R., Christensen, H. F., Trads, N., Hiorth, A., Madland, M. V., 2013. Measuring the Biot stress coefficient and its implications  
419 on the effective stress estimate. *Proc. 47th US Rock Mech./Geomech. Symposium*, San Francisco, CA, USA, ARMA, 282.
- 420 Nguyen, T. S., Selvadurai, A. P. S., Armand, G., 2005. Modelling the FEBEX THM experiment using a state surface approach. *International Journal*  
421 *of Rock Mechanics and Mining Sciences* 42, 639–651.
- 422 Pahl, A., Heusermann, S., Bräuer, V., Glögler, W., 1989. Grimsel Test Site. *Rock Stress Investigations*. Tech. rep., NAGRA Technical Report,  
423 88-39E, Baden, Switzerland.
- 424 Rabung, T., Molinero, J., Garcia, D., Montoya, V., 2012. 1st Workshop Proceedings of the Collaborative Project Crystalline Rock Retention  
425 Processes, (7th EC FP CP CROCK). KIT Scientific Publishing, Barcelona, Spain.
- 426 Redfern, S. A., Angel, R. J., 1999. High-pressure behaviour and equation of state of calcite, CaCO<sub>3</sub>. *Contributions to Mineralogy and Petrology*  
427 134 (1), 102–106.
- 428 Reuss, A., 1929. Berechnung der Fliegrenze von Mischkristallen auf Grund der Plastizitätsbedingung für Einkristalle. *Journal of Applied Mathe-*  
429 *matics and Mechanics* 9, 4958.
- 430 Rice, J. R., Cleary, M. P., 1976. Some basic stress diffusion solutions for fluidsaturated elastic porous media with compressible constituents.  
431 *Reviews of Geophysics and Space Physics* 14 (2), 227–241.
- 432 Rutqvist, J., Rejeb, A. M., T., Tsang, C.-F., 2003. Analyses of coupled hydrological-mechanical effects during drilling of the FEBEX tunnel at  
433 Grimsel. In O. Stephansson, J.A. Hudson and L. Jing (Eds), *Proceedings of GeoProc 2003 (Stockholm, 196 13-15.10.2003)* 44, 114–119.
- 434 Schaltegger, U., 1990a. Post-magmatic resetting of Rb-Sr whole rock ages - a study in the Central Aar Granite (Central Alps, Switzerland).  
435 *Geologische Rundschau* 79, 709–724.
- 436 Schaltegger, U., 1990b. The Central Aar Granite: highly differentiated calc-alkaline magmatism in the Aar Massif (Central Alps, Switzerland).  
437 *European Journal of Mineralogy* 2, 254–259.
- 438 Schaltegger, U., Corfu, F., 1992. The age and source of late Hercynian magmatization in the central Alps: evidence from precise U-Pb ages and  
439 initial Hf isotopes. *Contributions to Mineralogy and Petrology* 111, 329–344.
- 440 Schaltegger, U., Krähenbühl, U., 1990. Heavy rare earth element enrichment in granites of the Aar Massif (Central Alps, Switzerland). *Chemical*  
441 *Geology* 89, 49–63.
- 442 Schild, M., Siegesmund, S., Vollbrecht, A., Mazurek, M., 2001. Characterization of granite matrix porosity and pore-space geometry by in situ and  
443 laboratory methods. *Geophysical Journal International* 146, 111–125.
- 444 Schilling, F. R., Sinogeikin, S. V., Hauser, M., Bass, J. D., 2003. Elastic properties of model basaltic melt compositions at high temperatures.  
445 *Journal of Geophysical Research: Solid Earth* 108 (B6), 2304.
- 446 Selvadurai, A. P. S., 1996. *Mechanics of Poroelastic Media*. Kluwer Academic Publishers, The Netherlands.
- 447 Selvadurai, A. P. S., 2000. *Partial Differential Equations in Mechanics. Vol. 2. The Bi-harmonic Equation, Poissons equation*. Springer-Verlag,  
448 Berlin.
- 449 Selvadurai, A. P. S., 2004. Stationary damage modelling of poroelastic contact. *International Journal of Solids and Structures* 41 (8), 2043–2064.
- 450 Selvadurai, A. P. S., 2007. The Analytical Method in Geomechanics. *Applied Mechanics Reviews* 60 (3), 87–106.
- 451 Selvadurai, A. P. S., 2009. Influence of residual hydraulic gradients on decay curves for one-dimensional hydraulic pulse tests. *Geophysical Journal*  
452 *International* 177 (3), 1357–1365.
- 453 Selvadurai, A. P. S., 2018. The Biot coefficient for a low permeability heterogeneous limestone. *Continuum Mechanics and Thermodynamics*  
454 <https://doi.org/10.1007/s00161-018-0653-7>.
- 455 Selvadurai, A. P. S., Carnaffan, P., 1997. A transient pressure pulse method for the measurement of permeability of a cement grout. *Canadian Journal*  
456 *of Civil Engineering* 24 (3), 489–502.
- 457 Selvadurai, A. P. S., Glowacki, A., 2008. Evolution of permeability hysteresis of Indiana Limestone during isotropic compression. *Ground Water*  
458 46, 113–119.
- 459 Selvadurai, A. P. S., Glowacki, A., 2017. Stress-Induced Permeability Alterations in an Argillaceous Limestone. *Rock Mechanics and Rock*  
460 *Engineering* 50 (5), 1079–1096.





- 461 Selvadurai, A. P. S., Glowacki, A., 2018. Estimates for the local permeability of the Cobourg limestone. *Journal of Rock Mechanics and Geotechnical Engineering* 10 (6), 1009–1019.
- 462
- 463 Selvadurai, A. P. S., Letendre, A., Hekimi, B., 2011. Axial flow hydraulic pulse testing of an argillaceous limestone. *Environmental Earth Sciences* 64 (8), 2047–2058.
- 464
- 465 Selvadurai, A. P. S., Najari, M., 2015. Laboratory-scale hydraulic pulse testing: influence of air fraction in cavity on estimation of permeability. *Géotechnique* 65 (2), 126–134.
- 466
- 467 Selvadurai, A. P. S., Selvadurai, P. A., 2010. Surface permeability tests: Experiments and modelling for estimating effective permeability. *Proceedings of the Royal Society A: Mathematical, Physical and Engineering Sciences* 466 (2122), 2819–2846.
- 468
- 469 Selvadurai, A. P. S., Shirazi, A., 2004. Mandel-Cryer effects in fluid inclusions in damage-susceptible poroelastic geologic media. *Computers and Geotechnics* 31 (4), 285–300.
- 470
- 471 Selvadurai, A. P. S., Shirazi, A., 2005. An elliptical disc anchor in a damage-susceptible poroelastic medium. *International Journal for Numerical Methods in Engineering* 63 (14), 2017–2039.
- 472
- 473 Selvadurai, A. P. S., Suvorov, A. P., 2012. Boundary heating of poro-elastic and poro-elasto-plastic spheres. *Proceedings of the Royal Society A: Mathematical, Physical and Engineering Sciences* 468 (2145), 2779–2806.
- 474
- 475 Selvadurai, A. P. S., Suvorov, A. P., 2014. Thermo-poromechanics of a fluid-filled cavity in a fluid-saturated geomaterial. *Proceedings of the Physical Society A* 470, 20130634.
- 476
- 477 Selvadurai, A. P. S., Suvorov, A. P., 2016. *Thermo-poroelasticity and Geomechanics*. Cambridge University Press, Cambridge.
- 478
- 479 Selvadurai, A. P. S., Suvorov, A. P., Selvadurai, P. A., 2015. Thermo-hydro-mechanical processes in fractured rock formations during a glacial advance. *Geoscientific Model Development* 8 (7), 2167–2185.
- 480
- 481 Selvadurai, P. A., Selvadurai, A. P. S., 2014. On the effective permeability of a heterogeneous porous medium: The role of the geometric mean. *Philosophical Magazine* 94 (20), 2318–2338.
- 482
- 483 Sisodia, P., Verma, M. P., 1990. Polycrystalline elastic moduli of some hexagonal and tetragonal materials. *Physica Status Solidi* 122, 525–534.
- 484
- 485 Stalder, H. A., 1964. Petrographische und mineralogische Untersuchungen im Grimselgebiet. *Schweizerische Mineralogische und Petrographische Mitteilungen* 44, 187–398.
- 486
- 487 Steck, A., Burri, G., 1971. Chemismus und paragenesen von granaten und granitgneisen der Grünschiefer und amphibolitfazies der Zentralalpen. *Schweizerische Mineralogische und Petrographische Mitteilungen* 51, 534–538.
- 488
- 489 Talbot, D. R., Willis, J. R., Nesi, V., 1995. On improving the hashin-shtrikman bounds for the effective properties of three-phase composite media. *IMA Journal of Applied Mathematics (Institute of Mathematics and Its Applications)* 54 (1), 97–107.
- 490
- 491 Terzaghi, K., 1923. Die Berechnung der Durchlässigkeitsziffer des Tones aus dem Verlauf der Hydrodynamischen Spannungserscheinungen, *Akad. Wissensch. Wien Sitzungsber Mathnaturwissensch Klasse Iia* 142, 125–138.
- 492
- 493 Ting, T. C. T., 1996. *Anisotropic Elasticity: Theory and Applications*. Oxford University Press, Oxford.
- 494
- 495 Verruijt, A., 2015. *Theory and Problems of Poroelasticity*. Delft University of Technology, The Netherlands.
- 496
- 497 Voigt, W., 1928. *Lehrbuch der Kristallphysik*, B.G. Teubner. Leipzig.
- 498
- 499 Walpole, L., 1966. On bounds for the overall elastic moduli of inhomogeneous systems–I. *Journal of the Mechanics and Physics of Solids* 14, 151–162.
- 500
- 501 Wang, H. F., 2000. *Theory of Linear Poroelasticity with Applications to Geomechanics and Hydrogeology*. Princeton University Press, Princeton.
- 502
- 503 Wenning, Q. C., Madonna, C., de Haller, A., Burg, J. P., 2018. Permeability and seismic velocity anisotropy across a ductile brittle fault zone in crystalline rock. *Solid Earth* 9, 683–698.
- 504
- 505 Wüthrich, H., 1965. Rb-Sr-Altersbestimmungen am alpinen Berggraben Aarmassiv. *Schweizerische Mineralogische und Petrographische Mitteilungen* 45, 876–971.
- 506
- 507 Yue, Z. Q., Selvadurai, A. P. S., 1995. On the mechanics of a rigid disc inclusion embedded in a fluid saturated poroelastic medium. *International Journal of Engineering Science* 33 (11), 1633–1662.
- 508
- 509 Zhu, W., Hughes, J. J., Bicanic, N., Pearce, C. J., 2007. Nanoindentation mapping of mechanical properties of cement paste and natural rocks. *Materials Characterization* 58, 1189–1198.
- 510
- 511 Ziegler, M., Amann, F., 2012. Laboratory test results obtained from core samples from the Grimsel III borehole at Kessiturn. Tech. rep., Internal Report, Ingenieurgeologie, ETH Zurich.